Structural Determination of Bulk and Surface Tungsten Oxides with UV−vis Diffuse Reflectance Spectroscopy and Raman Spectroscopy

Elizabeth I. Ross-Medgaarden and Israel E. Wachs*

Operando Molecular Spectroscopy and Catalysis Laboratory, Department of Chemical Engineering, 111 Research Drive, Iacocca Hall, Lehigh University, Bethlehem, Pennsylvania 18015

Received: May 31, 2007; In Final Form: July 27, 2007

Combined UV−vis diffuse reflectance spectroscopy (DRS) and Raman spectroscopy were applied to examine the electronic and molecular structures, respectively, of well-defined W(VI) bulk mixed oxide reference compounds consisting of (i) isolated WO_4 or WO_6 monomers, (ii) dimeric $O_3W-O-WO_3$, (iii) polymeric chain of alternating WO_4/WO_6 units, and (iv) WO_6-coordinated W_9-W_{18} clusters. Raman spectroscopy was employed to confirm the identity and phase purity of the different tungsten oxide structures. UV−vis DRS provided the corresponding electronic edge energy (E_g) of the ligand-to-metal charge transfer (LMCT) transitions of the W(VI) cations. A correlation between the edge energy and the number of covalent bridging W−O−W bonds around the central W(VI) cation was found with E_g linearly decreasing with increasing number of bridging W−O−W bonds. However, a direct relationship between E_g and the domain size, N_W, for finite WO_x clusters does not exist. Subsequently, UV−vis and Raman spectroscopy information were applied to determine the local structures of the molecularly dispersed surface W(VI) species present in supported WO_3/Al_2O_3, WO_3/ZrO_2, and WO_3/SiO_2 catalysts under ambient and dehydrated conditions.

1. Introduction

Supported tungsten oxide catalytic materials are extensively used as heterogeneous catalysts for numerous petroleum, chemical, and environmental processes:[1−3] C_4-C_8 alkane isomerization (WO_3/ZrO_2),[4−10] hydrodesulphurization (HDS),[11] hydrocarbon cracking (WO_3/Al_2O_3),[12−15] olefin metathesis (WO_3/SiO_2),[16−19] and selective catalytic reduction of NO_x (WO_3/TiO_2).[20−23] Supported tungsten oxide catalysts have been extensively characterized in the literature with various spectroscopic techniques that provide molecular and electronic structural details as well as surface chemical characteristics.[6,9,10,24−32,90] The molecular and electronic structures of the surface WO_x species present in supported WO_3 catalysts, however, are still not completely resolved. Knowledge of the local structure of the surface tungsten oxide species plays an important role in the synthesis and optimization of supported tungsten oxide catalyst systems for targeted applications.

UV−vis diffuse reflectance spectroscopy (DRS) has increasingly been employed to investigate the local structure of W(VI) oxide compounds/mixed oxides,[33−34] W(VI) mesoporous materials,[35−36] W(VI) polyoxometalates,[37−39] and supported W(VI) catalysts.[6,10,35,40−47] In these investigations, the local structures of the W(VI) cation is often associated with the band positions of the ligand-to-metal charge transfer (LMCT) transitions in the ultraviolet, visible, and near-infrared regions. An important advantage of the UV−vis spectroscopic technique is its ability to function under ambient, dehydrated, and reaction conditions.[48−49]

Although the UV−vis DRS LMCT transitions tend to be quite broad, recent publications have indicated that the edge energy (E_g) of the LMCT transition can be quantified and contain information about the local structures of bulk and surface V(V) and Mo(VI) metal oxides.[50−52] Early studies by Weber[52] analyzed the UV−vis DRS edge energies of bulk molybdenum oxide samples from a number of different publications and found a correlation between the edge energy and the number of next nearest metal neighbors (N_M) of the Mo oxide compounds (Mo−O−Mo bonds), where *M* represents the degree of aggregation of the MoO_x structure. Analogous UV−vis DRS E_g−structure relationships have successfully been developed by Gao et al.[50] for oxides of vanadium and successfully applied for the local structural determination of the surface VO_x species present in supported V_2O_5 catalysts.

Several research groups[6,46−47,53] have extended Weber's methodology to also account for the domain size of the surface WO_x species present in supported WO_3 catalyst systems. No systematic examination between the UV−vis DRS E_g values and the number of covalent W−O−W bonds for tungsten oxide compounds, however, has been reported in the literature.

In the present investigation, UV−vis DRS is employed to establish a quantitative correlation between the number of covalent bridging W−O−W bonds in known bulk mixed metal tungstate and polyoxotungstate structures (isolated, polymeric, clusters, and bulk structures) and their corresponding edge energy (E_g).[9,10,54] This quantitative UV−vis DRS E_g−structure correlation, in conjunction with Raman spectroscopy, is subsequently employed to determine the local molecular structures of the surface tungsten oxide species present in the submonolayer surface coverage region on oxide supports (Al_2O_3, ZrO_2, and SiO_2) under ambient and dehydrated conditions. Unlike other spectroscopic techniques such as Raman and IR that give rise to sharp transitions, UV−vis DRS gives rise to broad bands that tend to overlap for multicomponent systems and only provide an average of the molecular-level characteristics. It is for this reason that complementary Raman and XANES data are required for a complete local structural determination of the

* To whom correspondence should be addressed. Phone: (610) 758-4274. Fax: (610) 758-6555. E-mail: iew0@lehigh.edu.

10.1021/jp074219c CCC: $37.00
Published on Web 09/22/2007

TABLE 1: Bulk Tungstate Reference Compounds

bulk tungstate compound	manufacturer
aluminum tungstate, $Al_2(WO_4)_3$	Alfa Aesar, 99%
ammonium metatungstate, $(NH_4)_6H_2W_{12}O_{40}$	Pfaltz & Bauer, Inc, 99.5%
ammonium paratungstate, $(NH_4)_{10}H_2W_{12}O_{42}$	H.C. Starck, 99%
calcium tungstate, $CaWO_4$	Alfa Aesar, 99%
magnesium tungstate, $MgWO_4$	Alfa Aesar, 99.5%
nickel tungstate, $NiWO_4$	Alfa Aesar, 99%
phosphotungstic acid, $H_3PW_{12}O_{40}\cdot xH_2O$	Aldrich, 99%
potassium tungstate, K_2WO_4	Alfa Aesar, 99.5%
silicotungstic acid, $H_4SiW_{12}O_{40}\cdot xH_20$	Aldrich, 99%
sodium 12-tungstophosphate, $Na_3PW_{12}O_{40}$	Strem Chemicals, 99%
sodium tungstate, Na_2WO_4	Alfa Aesar, 98%
tungsten(VI) oxide, WO_3	Alfa Aesar, 99.8% (metals basis)
tungsten zirconia, $Zr(WO_4)_2$	Alfa Aesar, 99.7%
zinc tungstate, $ZnWO_4$	Alfa Aesar, 99.7%

surface tungsten oxide species on oxide supports under ambient and dehydrated conditions.

2. Experimental Section

Catalyst Preparation. Most of the bulk tungsten oxide compounds in this study were obtained from commercial suppliers indicated in Table 1, and the compounds were used as received. The bulk metal tungstates of MgW_2O_7, $Na_2W_2O_7$, and $K_2W_2O_7$ were prepared by coprecipitation of aqueous ammonium metatungstate, $(NH_4)_{10}W_{12}O_{41}\cdot 5H_2O$ (Pfaltz & Bauer, 99.5% purity), and the corresponding metal nitrates ($Mg(NO_3)_2\cdot 6H_2O$, $NaNO_3$, and KNO_3, Alfa Aesar, 99.9%) with synthesis methods previously reported.[55,56,67] Molecular heteropolyoxotungstate Keggin and Wells-Dawson clusters containing W_9−W_{18} atoms ($Na_9HSiW_9O_{34}\cdot 23H_2O$,[57] $H_6P_2W_{18}O_{62}\cdot 24H_2O$,[58−59] α-$K_{10}P_2W_{17}O_{61}\cdot 15H_2O$,[60−61] and α/β-$K_6P_2W_{18}O_{62}\cdot 10H_2O$[60−61]) were synthesized by methods previously described.

The oxide supports used for this study were Al_2O_3 (Engelhard, $S_{BET} \approx 200$ m^2/g), ZrO_2 (Degussa, $S_{BET} = 60$ m^2/g), and SiO_2 (Cabosil EH-5, $S_{BET} \approx 330$ m^2/g). The supported tungsten oxide catalysts were prepared by incipient-wetness impregnation of aqueous solutions of ammonium metatungstate, $(NH_4)_{10}W_{12}O_{41}\cdot 5H_2O$ (Pfaltz & Bauer, 99.5% purity), into the various supports to achieve 1/8 and 1 monolayer surface coverage. The samples were dried overnight under ambient conditions and subsequently dried in flowing air (Airgas, Zero Grade) at 120 °C for 1 h and calcined in flowing air (Airgas, Zero Grade) at 450 °C for 4 h. The following notation is employed to express the supported tungsten oxide samples: *x*WSupport, where *x* is the surface density (W-atoms/nm^2) and Support is the support (i.e., 4.5WZr represents a surface density of 4.5 W/nm^2 for the supported WO_3/ZrO_2 catalyst). Surface tungsten oxide coverage and loading for the supported WO_3 catalysts are found in Table 2.

Raman Spectroscopy. Raman spectroscopy was used to obtain the molecular structures of the bulk and supported tungsten oxide catalysts with either a visible (532 nm; bulk tungstates, ZrO_2- and SiO_2-supported WO_3) or an ultraviolet (325 nm; Al_2O_3-supported WO_3) laser excitation on a single-stage Horiba-Jobin Yvon Lab Ram-HR Raman spectrometer equipped with a confocal microscope (Olympus BX-30) and a notch filter (Kaiser Super Notch). The visible excitation was generated by a Nd−YAG doubled diode pumped laser (Coherent Compass 315M-150; output power of 150 mW with sample power 10 mW), and the UV laser excitation was generated from a He−Cd laser (Kimmon model IK5751I-G; output power of 30 mW with sample power ≈ 7 mW). The scattered photons were directed into a single monochromator and focused onto a UV-sensitive liquid-N_2-cooled CCD detector (Horiba-Jobin Yvon CCD-3000V) with a spectral resolution of ∼2 cm^{-1} for the given parameters. The Raman spectrometer was also equipped with an environmentally controlled high-temperature cell reactor (Linkam, TS1500) that examined the catalyst samples in loose powder form (∼5−10 mg) and also allowed for control of both the temperature and gaseous composition. The Raman spectra of the ambient supported tungsten oxide catalysts were collected before the samples were dehydrated. *In situ* Raman spectra were collected for the supported tungsten oxide catalysts after dehydration at 450 °C for 1 h in flowing 10% O_2/He (Airgas, certified, 9.735% O_2/He, ultrahigh purity and hydrocarbon free, 30 mL/min) to desorb the adsorbed moisture, and the spectra of the dehydrated samples were collected after cooling the catalysts back to room temperature in the flowing 10% O_2/He gas. The Raman spectra of the bulk tungsten oxide compounds were taken under ambient conditions. The spectral acquisition time employed was 20 scans of 20 s/scan for a total of ∼7 min/spectrum.

TABLE 2: Surface Tungsten Oxide Coverage and Loading for the Supported WO_3 Catalysts

catalyst	surface area of support (m^2/g)	surface density (W atoms/nm^2)	% of monolayer coverage
WO_3/ZrO_2	60	0.5	0.13
		4.5	1
WO_3/Al_2O_3	∼200	0.5	0.13
		4.5	1
WO_3/SiO_2	∼330	∼0.1 (1%)	*a*
		∼0.5 (6%)	*a*

[a] Monolayer surface coverage for the supported WO_3/SiO_2 catalyst system is not achievable. Maximum dispersion before crystalline WO_3 formation is ∼6% WO_3/SiO_2.

UV−vis Diffuse Reflectance Spectroscopy (DRS). The electronic structures of the bulk tungsten oxide reference compounds and the supported tungsten oxide catalysts were obtained with a Varian Cary 5E UV−vis spectrophotometer employing the integration sphere diffuse reflectance attachment (Harrick Praying Mantis Attachment, DRA-2). The finely ground powder samples (∼20 mg) of the bulk tungstate reference compounds and the supported tungsten oxide catalysts were loaded into an *in situ* cell (Harrick, HVC-DR2) and measured in the 200−800 nm region with a magnesium oxide reflectance standard used as the baseline. The UV−vis spectra of the bulk tungstate reference compounds were obtained under ambient conditions, and the spectra of the supported tungsten oxide catalysts were obtained after the samples were treated at 400 °C for 1 h in flowing 10% O_2/He (Airgas, certified, 9.735% O_2/He, ultrahigh purity and hydrocarbon free, 30 mL/min) to desorb the adsorbed moisture. Below 300 nm, the absorbance signal was unacceptably noisy and a filter (Varian, 1.5ABS) was employed to minimize the background noise. For the UV−vis DRS studies of the supported tungsten oxide catalysts in the present work, absorption from the Al_2O_3 and SiO_2 supports can be neglected as compared to the strong absorption of the W(VI) cations. The ZrO_2 support, however, exhibits strong absorption in the UV−vis region and, thus, cannot be neglected. Therefore, the Al_2O_3, ZrO_2, and SiO_2 supports were used as the baseline for the supported tungsten oxide catalysts to keep all the systems consistent.

The UV−vis spectra were processed with Microsoft Excel software, consisting of calculation of the Kubelka−Monk function, $F(R_\infty)$, which was extracted from the UV−vis DRS absorbance. The edge energy (E_g) for allowed transitions was determined by finding the intercept of the straight line in the

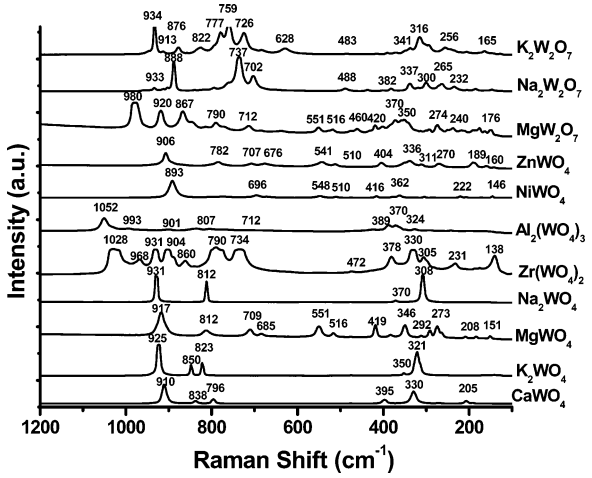

Figure 1. Raman spectra (532 nm) of bulk tungstate reference compounds.

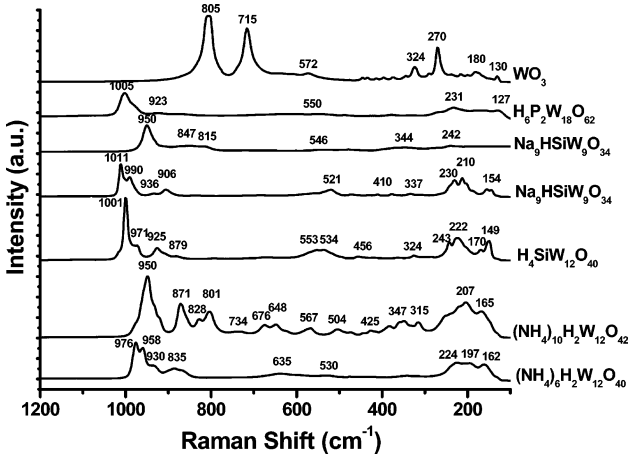

Figure 2. Raman spectra (532 nm) of heteropolyoxo tungstates and bulk WO_3.

low-energy rise of a plot of $[F(R_\infty)h\upsilon]^{1/n}$, where $n = 0.5$ for the direct allowed transition, vs $h\upsilon$, where $h\upsilon$ is the incident photon energy.[50,62,63]

3. Results

3.1. Bulk Tungsten Oxide Compounds. The Raman spectra of bulk tungsten oxide reference compounds, under ambient conditions, are presented in Figures 1 and 2. The absence of characteristic WO_3 vibrations at 805, 715, and 270 cm^{-1} demonstrates the phase purity of these tungstate reference compounds. The corresponding UV−vis DRS band maxima and edge energy values are provided in Table 3. The UV−vis DRS spectra of selected bulk tungstates are shown in Figure 3, which illustrates the various locations of the ligand-to-metal charge transfer (LMCT) transition of different tungsten oxide structures (Figure 3A) and the determination of edge energy from the UV−vis spectra for selected compounds (Figure 3B).

Isolated WO_4 Structures. Various bulk crystalline orthotungstate compounds possessing isolated WO_4 sites are known (i.e., $CaWO_4$, Na_2WO_4, K_2WO_4, $Al_2(WO_3)_4$, and $Zr(WO_4)_2$, etc.);[64,66] unfortunately, an ideal WO_4 structure has not been found. Hardcastle et al.,[64] using the diatomic approximation method, concluded that for an ideal WO_4 unit the shortest W−O bond should correspond to a Raman fingerprint located at 874 cm^{-1} (ν_s(W═O)), with a standard deviation of approximately 55 cm^{-1}. It is expected for compounds consisting of WO_4 units that the υ_s vibration will shift to higher wavenumber values as the W−O bond is shortened by distortions.[64] The tungstate ion in aqueous solution, $[WO_4]_{aq}^{2-}$, exhibits Raman vibrations at 931 (ν_s(W═O)), 834 (ν_{as}(W═O)), and 326 (δ(W═O)) cm^{-1}.[64,69,75] The shortest W−O bond in the aqueous tungstate ion exhibits a Raman stretching mode at 931 cm^{-1} revealing that the $[WO_4]_{aq}^{2-}$ ion is significantly distorted from the ideal tetrahedron because it is hydroxylated.[64] Bulk $CaWO_4$, which has a scheelite structure, exhibits Raman bands at 910, 838, 796, 395, 330, and 205 cm^{-1},[30] revealing its slightly distorted isolated WO_4 unit. Bulk Na_2WO_4 consists of a spinel WO_4-coordinated structure and exhibits Raman bands at 931, 812, 370, and 308 cm^{-1}.[30] The Raman spectrum of the isolated WO_4 sites in bulk K_2WO_4 possesses bands at 925, 850, 823, 350, and 321 cm^{-1}. The bulk $CaWO_4$, K_2WO_4, and Na_2WO_4 crystalline compounds exhibit a single strong Raman band in the 910−931 cm^{-1} region from the ν_s(W═O) vibration, reflecting the presence of only one slightly irregular WO_4 unit in these reference compounds. The absence of Raman bands in the 500−700 cm^{-1} region reflects the absence of bridging W−O−W bonds in the above structures.

Bulk $Al_2(WO_4)_3$ and $Zr(WO_4)_2$ are more complex tungstates since they contain multiple WO_4 sites that are highly distorted. Crystalline $Al_2(WO_4)_3$ possesses a garnet structure consisting of both regular and distorted WO_4 groups that give rise to major Raman bands at 1052, 993, 901, 807, 712, 389, 370, and 324 cm^{-1}.[30] The bulk $Zr(WO_4)_2$ cubic structure exhibits the main Raman features at 1028, 968, 931, 904, 860, 790, 734, 378, 330, 305, 231, and 138 cm^{-1}. The appearance of multiple Raman bands in the 900−1060 cm^{-1} range for bulk $Al_2(WO_4)_3$ and $Zr(WO_4)_2$ indicates that these structures contain more than one isolated WO_4 unit. The presence of isolated WO_4 structures in these orthotungstate reference compounds is confirmed by the absence of Raman features in the 500−700 cm^{-1} range characteristic of bridging W−O−W bonds.

A unique feature of UV−vis DRS for the isolated WO_4 reference compounds is that they only possess a single ligand-to-metal charge transfer (LMCT) band in the general region of ∼218−274 nm, with many of the band maxima occurring at ∼220−250 nm. The exact location of this band maximum depends on the extent of distortion of the isolated WO_4 structure. For example, K_2WO_4 has a relatively undistorted isolated WO_4 unit and possesses a LMCT band at ∼223 nm, whereas $Zr(WO_4)_2$ consists of a distorted isolated WO_4 unit and exhibits a LMCT band at ∼274 nm. The corresponding UV−vis DRS E_g values for the more regular WO_4 structures are 5.2−5.6 eV and 4.0−4.2 eV for the highly distorted WO_4 structures.

Isolated WO_6 Structures. A perfect undistorted isolated WO_6 structure has not been found. Hardcastle et al.,[64] using the diatomic approximation method, concluded that for an ideal WO_6 unit the shortest W−O bond should correspond to a Raman band located at 691 cm^{-1} (ν_s(W═O)) with a standard deviation of approximately 55 cm^{-1}. It is expected for compounds consisting of WO_6 units that the υ_s vibration will shift to higher wavenumber values as the W−O bond is shortened by distortions.[64] The aqueous ion containing an isolated WO_6 structure is predicted to give rise to Raman bands at 740 (ν_s(W═O)), 430 (ν_{as}(W═O)), and 360 (δ(W═O)) cm^{-1}.[64,69] Unlike an ideal WO_4 structure where all four normal vibrational modes of the tetrahedral structure are Raman active, an ideal WO_6 structure has six normal modes of vibration of which only three are Raman active.[65] The isolated WO_6 wolframite structure is found in the bulk crystalline $NiWO_4$ and $ZnWO_4$[66−67] reference compounds. Bulk $NiWO_4$ possesses Raman features at 893, 696, 548, 510, 416, 362, 305, 222, and 146 cm^{-1}, where the band at

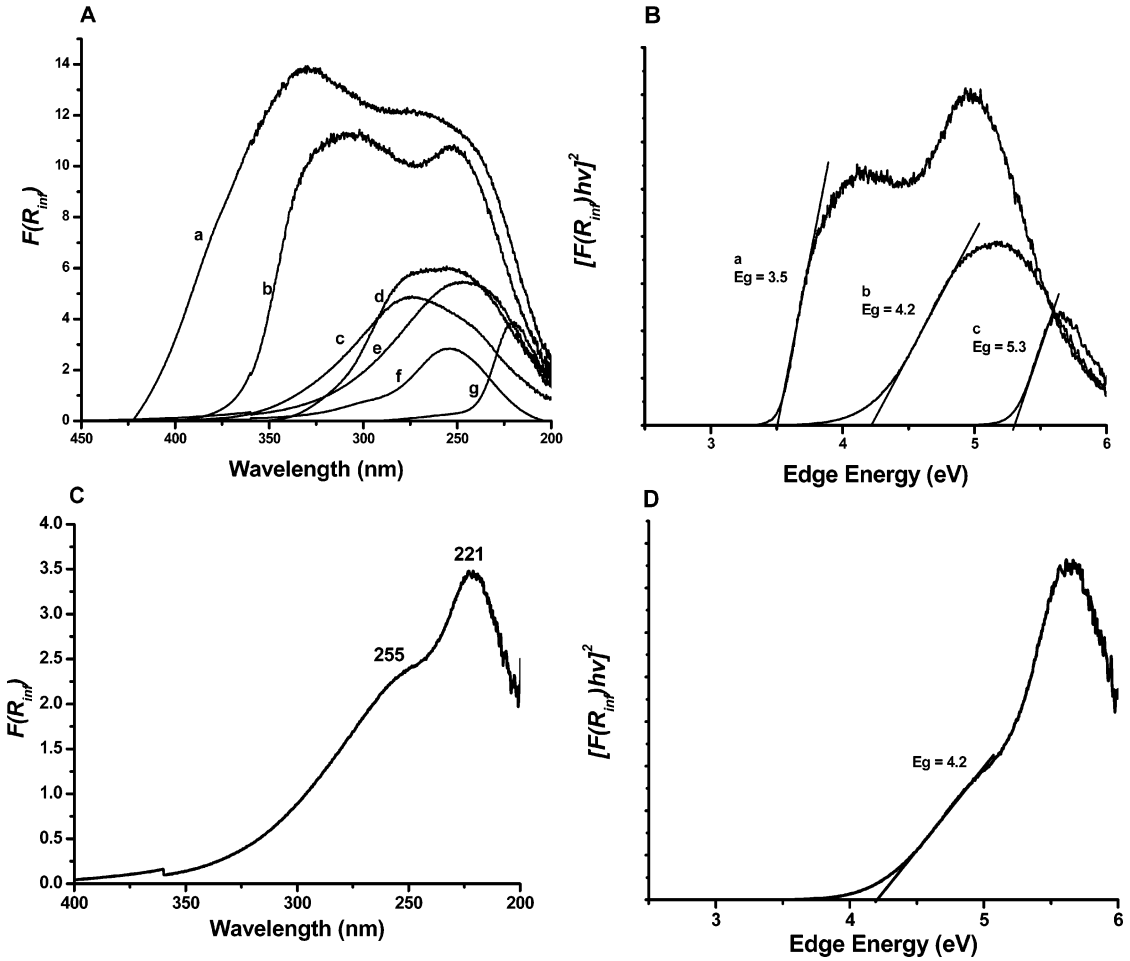

Figure 3. (A) UV−vis DRS spectra of selected bulk tungstate reference compounds: (a) WO_3, (b) $(NH_4)_6H_2W_{12}O_{40}$, (c) $Al_2(WO_4)_3$, (d) $Na_2W_2O_7$, (e) $Zr(WO_4)_2$, (f) MgW_2O_7, and (g) Na_2WO_4. (B) UV−vis DRS spectra and E_g values of selected bulk tungstate reference compounds: (a) $(NH_4)_6H_2W_{12}O_{40}$, (b) $Al_2(WO_4)_3$, and (c) Na_2WO_4. (C) UV−vis DRS spectra and LMCT transition bands of a 50/50 physical mixture of $Al_2(WO_4)_3$ and Na_2WO_4. (D) UV−vis DRS spectra and E_g values of a 50/50 physical mixture of $Al_2(WO_4)_3$ and Na_2WO_4.

TABLE 3: Local WO_x Structure and Corresponding UV−vis DRS Edge Energy (E_g) Values of Bulk Tungsten Oxide Reference Compounds

catalyst system	band max (nm)	E_g (eV)	mol struct
$CaWO_4$	218(sh), 256	5.6	isolated WO_4
Na_2WO_4	218, 258 (w)	5.3	isolated WO_4
K_2WO_4	223	5.2	isolated WO_4
$MgWO_4$	218(sh), 320	5.2	isolated WO_4
$Al_2(WO_4)_3$	250	4.2	distorted, isolated WO_4
$Zr(WO_4)_2$	274	4.0	distorted, isolated WO_4
$NiWO_4$	247(sh), 342	4.5	distorted, isolated WO_6
$ZnWO_4$	270(w), 344	4.5	distorted, isolated WO_6
MgW_2O_7	252, 296 (w)	4.3	dimeric $O_3W-O-WO_3$
$Na_2W_2O_7$	250, 270(w)	4.1	infinite chain, alternating WO_4/WO_6
$K_2W_2O_7$	252, 306(w)	3.6	infinite chain, alternating WO_4/WO_6
$Na_9HSiW_9O_{34}$	250, 294(sh)	3.7	WO_6-containing cluster
$(NH_4)_{10}H_2W_{12}O_{42}$	269,314	3.6	WO_6-containing cluster
$(NH_4)_6H_2W_{12}O_{40}$	254, 318	3.5	WO_6-containing cluster
α_2-$K_{10}P_2W_{17}O_{61}\cdot 15H_2O$	290	3.4	WO_6-containing cluster
$H_4SiW_{12}O_{40}$	254, 323	3.4	WO_6-containing cluster
$H_3PW_{12}O_{40}\cdot 24H_2O$	254, 306	3.4	WO_6-containing cluster
$Na_3PW_{12}O_{40}$	255, 328	3.4	WO_6-containing cluster
α-$K_6P_2W_{18}O_{62}\cdot 10H_2O$	257(sh), 302, 345, 372(sh)	3.1	WO_6-containing cluster
$H_6P_2W_{18}O_{62}\cdot 24H_2O$	255(sh), 300(w), 356, 384	3.0	WO_6-containing cluster
WO_3	251, 330	2.8	infinite 3D WO_6 structure

893 cm^{-1} is associated with the WO_6 symmetric stretching vibration. Bulk $ZnWO_4$ exhibits Raman bands at 906, 782, 707, 676, 541, 510, 404, 336, 311, 270, 189, and 160 cm^{-1}, with the 906 cm^{-1} band representing the symmetric stretch. Both crystalline WO_6 structures are distorted, which is reflected in the Raman shift from 691 to 893−906 cm^{-1} for the symmetric stretch. The corresponding UV−vis DRS E_g values are ~4.5 eV with the LMCT band maxima between 247−252 and 342−344 nm, which reflect the distorted nature of the isolated WO_6 units present in these bulk tungstate reference compounds.

Dimeric W_2O_7 Structure. Bulk tungsten oxide compounds rarely form polymeric WO_4 compounds with the exception of

MgW_2O_7 that consists of a pair of sharing WO_4 tetrahedra (dimeric $O_3W-O-WO_3$ unit).[66] The Raman bands of bulk MgW_2O_7 appear at 980, 920, 967, 790, 712, 551, 516, 420, 370, 350, 274, 240, and 176 cm^{-1}. The 980 cm^{-1} vibration represents the $\nu_s(W=O)$, the vibrations in the 500−800 cm^{-1} range represent $\nu_s(W-O-W)$ and $\nu_{as}(W-O-W)$, and the $\delta(W=O)$ and $\delta(W-O-W)$ bending modes occur in the 200−400 cm^{-1} range. Two LMCT band maxima at 252 and 296 (w) nm are present in the UV−vis spectrum of MgW_2O_7. The corresponding UV−vis DRS E_g value of 4.3 eV is slightly lower than that found in the isolated WO_4 or WO_6 bulk compounds with the exception of the highly distorted isolated WO_4 structures.

Polymeric W_2O_7 Linear Chain. Bulk disodium tungstate, $Na_2W_2O_7$, and dipotassium tungstate, $K_2W_2O_7$, are composed of alternating WO_4 and WO_6 units joined to give an infinite polymeric chain.[30] The Raman band at 934−933 cm^{-1} is assigned to the symmetric W=O stretching mode of the WO_4 site, and the band at 888−876 cm^{-1} is assigned to the symmetric W=O stretching mode of the WO_6 site. The stretching and bending modes of the bridging W−O−W infinite chain appear at ∼500−800 and ∼200−300 cm^{-1}, respectively.[30] The UV−vis spectrum of $Na_2W_2O_7$ gives rise to two LMCT bands with maxima at 250 and 270 nm, and the UV−vis spectrum of $K_2W_2O_7$ also gives rise to two LMCT bands with maxima at 252 and 306 nm. The corresponding UV−vis DRS E_g values for $Na_2W_2O_7$ and $K_2W_2O_7$ of 4.1 and 3.6 eV, respectively, are lower than that found in the dimeric $O_3W-O-WO_3$ structure as well as the isolated WO_4 or WO_6 reference compounds. The E_g value for $Na_2W_2O_7$, however, exhibits a comparable E_g value also found for highly distorted and isolated WO_4 structures (i.e., $Al_2(WO_4)_3$ and $Zr(WO_4)_2$), whereas the E_g value for $K_2W_2O_7$ lies much lower.

$W_{12}O_x-W_{18}O_x$ Clusters. Tungsten oxide clusters composed of polymeric WO_6 units are found in ammonium tungstates as well as Wells-Dawson and Keggin heteropolytungstate compounds. Ammonium metatungstate, $[W_{12}O_{42}]^{12-}$, possesses significantly distorted WO_6 units and exhibits Raman features at ∼976 ($\nu_s(W=O)$), 958, 930, 834 ($\nu_{as}(W=O)$), and W−O−W modes at 700−500 and 330−190 cm^{-1}. The Keggin heteropolyoxo anions consist of polymeric $W_{12}O_{40}$ clusters with the general formula of $[XW_{12}O_{40}]^{3-}$. The Keggin anion's general structure is composed of a globe-like cluster of corner and edge-sharing WO_6 units that enclose a central XO_4 unit (where X represents P, Si, etc.). The tungsten WO_6 units possess one short W=O bond, four W−O−W bonds, and one long W−O−X bond to the central XO_4 unit. The Raman spectra of the Keggin anions exhibit bands between 950 and 1015 cm^{-1} ($\nu_s(W=O)$) and 825−930 cm^{-1} ($\nu_{as}(W=O)$) as well as bands at lower wavenumbers arising from the bridging W−O−W bonds. The larger Wells-Dawson heteropoly anions, (i.e., α-$[X_2W_{18}O_{62}]^{6-}$) and Wells-Dawson lacunary species (i.e., α_2-$[X_2W_{17}O_{61}]^{10-}$) exhibit multiple W=O vibrations between 950 and 1005 cm^{-1}, reflecting a distribution of distortions among the WO_6 units in the framework.

The corresponding UV−vis DRS E_g values for these reference isopolytungstates occur between 3.0 and 3.6 eV, which is much lower than any of the previous tungsten oxide reference compounds. These isopolytungstate compounds contain multiple LMCT transitions which differ slightly depending on the parent ion. For the Keggin compounds with the general formula $[XW_{12}O_{40}]^{3-}$, two LMCT transitions occur between 250−269 and 294−328 nm. The larger Wells-Dawson heteropoly anions, (i.e., α-$[X_2W_{18}O_{62}]^{6-}$) possess a single LMCT transition at 290 nm, where the Wells-Dawson lacunary species (i.e., α_2-$[X_2W_{17}O_{61}]^{10-}$) exhibit four LMCT transitions between 247 and 257, ∼300, 345−356, and 372−384 nm. Furthermore, the position of the UV−vis DRS band maxima and the E_g values of the Keggins are independent of the central cation (Si or P) as well as the charge-balancing secondary cation (H^+ or Na^+).

Infinite 3D Structure. Crystalline WO_3 is a three-dimensional structure composed of distorted WO_6 units that exhibits major Raman bands at 805, 715, and 270 cm^{-1}. The 805 and 715 cm^{-1} vibrations arise from the bridging W−O−W stretching frequencies, and the 270 cm^{-1} vibration is the related bridging W−O−W bending mode.[30,69] Bulk WO_3 contains two LMCT transitions at 251 and 338 nm with the corresponding UV−vis DRS E_g value of 2.8 eV which is even lower than that found for the finite clusters present in the Keggin and Wells-Dawson reference compounds. Crystalline WO_3 nanoparticles (NPs) give rise to strong Raman bands,[27] and the absence of these bands in the tungsten oxide reference compounds reflects their phase purity.

Summary of UV−vis and Raman Spectroscopy of Bulk Tungstates. The extensive set of UV−vis and Raman spectra in Figures 1 and 2 and Table 3 reveal several trends between tungstate structures and their spectra. Raman spectroscopy is sensitive to (i) the number of distinct WO_x sites in a structure (reflected in the number of symmetric bands in the high wavenumber region), (ii) the extent of distortion of the local WO_x structure (shift in symmetric stretch relative to ideal structures), and (iii) the presence of the polytungstate functionality (W−O−W). Furthermore, the Raman bands tend to be sharp, and the molecular nature of Raman spectroscopy sometimes allows identification of specific structures when appropriate reference compounds are available. A minor downside of Raman spectroscopy is that it is more sensitive to species possessing higher W−O bond order (i.e., W=O vs W−O).

The UV−vis spectra allow for discrimination between mildly distorted isolated WO_4/WO_6 ($E_g > 4.4$ eV) and polymeric structures ($E_g < 4.0$ eV). The number and location of LMCT transition band maxima further discriminates between these structures since isolated WO_4 units generally result in only one strong transition occurring at ∼220 nm, whereas slightly distorted monotungstate structures and polytungstates, especially clusters, tend to give rise to multiple strong LMCT bands between 250 and 350 nm. In the region 4.0 eV $< E_g <$ 4.4 eV, however, several types of tungstate compounds possess E_g values that complicate UV−vis structural assignments. For example, highly distorted WO_4 sites give rise to E_g values of 4.0−4.2 eV with an LMCT of ∼250−270 nm, the dimeric W_2O_7 unit exhibits an E_g value of 4.3 eV with LMCT of ∼250 nm, and polytungstate W_2O_7 chains can also yield an E_g value of 4.1 eV with an LMCT of ∼250 nm.

A further complication of UV−vis spectral analysis can result when multiple structures are present in the same sample because of the broadness of the bands. For example, if a mixture contains comparable quantities of both mildly distorted WO_4 species (Na_2WO_4 with $E_g \approx 5.3$ eV and LMCT ≈ 218 nm) and highly distorted WO_4 species ($Al_2(WO_4)_3$ with $E_g \approx 4.2$ eV and LMCT ≈ 250 nm), the resulting UV−vis spectrum is dominated by the lower E_g value of the highly distorted WO_4 species and exhibits two LMCT band maxima at 218 and 255 nm (see Figure 3C). Note that the apparent E_g value of the $Na_2WO_4/Al_2(WO_4)_3$ physical mixture is dominated by the lower E_g value of the highly distorted WO_4 site present in $Al_2(WO_4)_3$, but the LMCT transition gives rise to the two bands from the individual Na_2WO_4 and $Al_2(WO_4)_3$ structures. A similar result would occur if

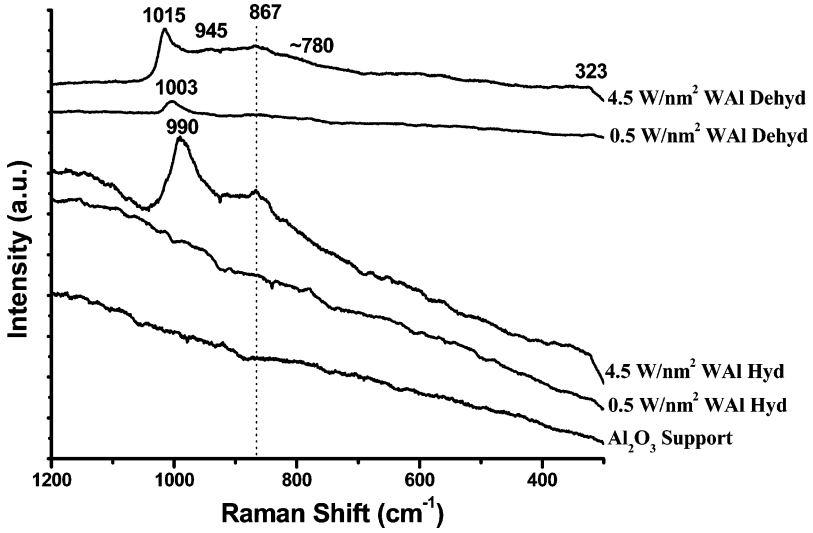

Figure 4. Raman spectra (325 nm) of supported WO_3/Al_2O_3 catalysts under ambient and dehydrated conditions as a function of surface tungsten oxide coverage (W/nm^2).

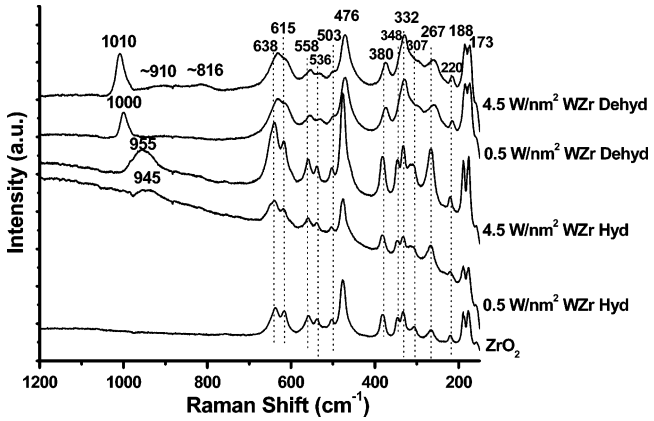

Figure 5. Raman spectra (325 nm) of supported WO_3/ZrO_2 catalysts under ambient and dehydrated conditions as a function of surface tungsten oxide coverage (W/nm^2).

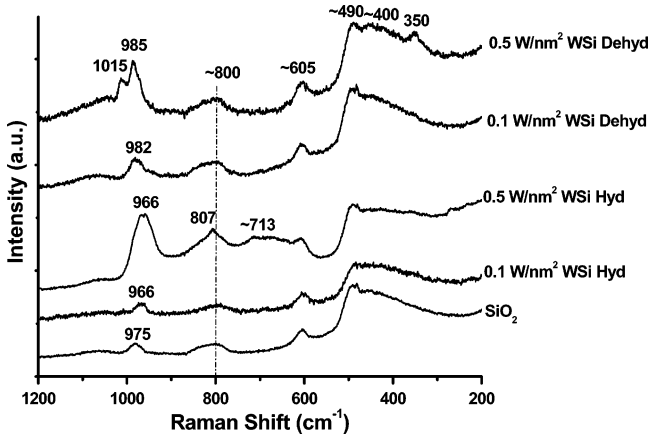

Figure 6. Raman spectra (532 nm) of supported WO_3/SiO_2 catalysts under ambient and dehydrated conditions as a function of surface tungsten oxide coverage (W/nm^2).

a sample has comparable amounts of monotungstate and polytungstate components. For multicomponent tungstate systems, thus, the overall E_g value is dominated by the component with lowest E_g values and the LMCT transition of each component is retained. The broad nature of the UV−vis LMCT bands, however, sometimes complicates detection of each individual LMCT transition in mixed tungstate structures. It is, thus, critical that both Raman and UV−vis spectra be collected on the same sample and under the same experimental conditions to obtain a more complete perspective of the components in tungstate mixtures.

3.2. Supported Tungsten Oxide Catalysts. The surface tungsten oxide coverage and loading for the examined supported WO_3 catalysts are summarized in Table 2. Monolayer surface coverage for Al_2O_3 and ZrO_2 is ∼4.5 W atoms/nm^2.[40,70,71] The maximum dispersion achieved for the supported WO_3/SiO_2 catalyst is ∼0.5 W atoms/nm^2 since higher tungsten oxide loadings resulted in the presence of crystalline WO_3 NPs. The Raman spectra under ambient and dehydrated conditions of the supported WO_3 catalysts are shown in Figures 4−6, and the corresponding UV−vis DRS edge energies and LMCT transitions are listed in Tables 4 and 5.

Supported WO_3/Al_2O Catalysts. The Raman spectra of the supported WO_3/Al_2O_3 catalysts under ambient and dehydrated conditions are presented in Figure 4. The Al_2O_3 support does not give rise to any Raman vibrations, which allows detection of all of the W−O vibrations. Raman bands from crystalline WO_3 NPs (805, 715, 270 cm^{-1}) are not present and confirm the successful complete dispersion of the tungsten oxide phase over the Al_2O_3 support at high and low surface coverage. Under ambient conditions, Raman bands are present at ∼990 cm^{-1} ν_s(W═O) and ∼867 cm^{-1} ν_{as}(W═O) for the hydrated monolayer supported 4.5WAl sample that are characteristic of the hydrated $[W_{12}O_{39}]^{6-}$ cluster that possesses Raman bands at ∼990−960 cm^{-1} (ν_s(W═O)) and 330−190 cm^{-1} (W−O−W mode).[31,74] Sample fluorescence prevented collection of the Raman spectra for the low-coverage supported 0.5WAl catalyst under ambient conditions, but a previous Raman analysis of supported ∼0.5WAl catalyst under ambient conditions exhibited bands at 951, 880, and 330 cm^{-1}.[31] These vibrations are characteristic of distorted aqueous $[WO_4]^{2-}$ monotungstate.[31] Upon dehydration, the major Raman bands from the dehydrated surface WO_x species appear at ∼1001 and 1015 cm^{-1} for the supported 0.5 and 4.5WAl catalysts, respectively. The monolayer supported 4.5WAl catalyst contains additional Raman bands at ∼867, ∼780, and ∼323 cm^{-1} assigned to the symmetric stretch of the bridging W−O−Al bond, asymmetric stretch of the bridging W−O−W bond, and associated O−W−O bending mode of the dehydrated surface WO_x species, respectively.[29,30,72] The short W═O bonds at ∼1001 and ∼1015 cm^{-1} are

TABLE 4: Comparison of UV−vis DRS Local WO_x Molecular Structural Assignments for Supported WO_3 Catalysts with Raman and XANES under Ambient Conditions

				local WO_x structural assignments under ambient conditions		
catalyst system	band max (nm)	E_g (eV)	average no. W−O−W bonds	UV−vis DRS	Raman	XANES
0.5 W/nm^2 WO_3/Al_2O_3	227	5.3	∼0	monotungstate (WO_4)	monotungstate ($[WO_4]^{2-}$) [31]	distorted WO_4[30,77]
4.5 W/nm^2 WO_3/Al_2O_3	228, 254	4.1	2.2	combination of mono- and polytungstates	polytungstate $[W_{12}O_{39}]^{6-}$cluster	distorted WO_5/WO_6[30,77]
0.5 W/nm^2 WO_3/ZrO_2	226, 249	4.6	1.1	monotungstate	monotungsate $[WO_4]^{2-}$	distorted WO_4[30,76,77]
4.5 W/nm^2 WO_3/ZrO_2	221, 249, 266 (sh)	4.3	1.6	combination of mono- and polytungstates	polytungstate $[HW_6O_{21}]^{5-}$ cluster	distorted WO_5/WO_6[30,76,77]
∼0.1 W/nm^2 WO_3/SiO_2	224, 260	4.2	2.0	combination of mono- and polytungstates	polytungstate $[W_{12}O_{39}]^{6-}$cluster	Si-containing Keggin-type cluster
∼0.5 W/nm^2 WO_3/SiO_2	222, 260	4.2	2.1	combination mono- and polytungstates	polytungstate $[W_{12}O_{39}]^{6-}$cluster and trace of WO_3 NPs	Si-containing Keggin-type cluster

TABLE 5: Comparison of UV−vis DRS Local WO_x Molecular Structural Assignments for Supported WO_3 Catalysts with Raman and XANES under Dehydrated Conditions

				local WO_x structural assignments under dehydrated conditions		
catalyst system	band max (nm)	E_g (eV)	average no. W−O−W bonds	UV−vis DRS	Raman	XANES
0.5 W/nm^2 WO_3/Al_2O_3	228	5.1	∼0	monotungstate	monotungstate (monoxo WO_5)	distorted WO_4[30,77]
4.5 W/nm^2 WO_3/Al_2O_3	234, 254	4.0	2.5	combination of mono- and polytungstates	polytungstate (monoxo WO_5/WO_6)	distorted WO_5/WO_6[30,77]
0.5 W/nm^2 WO_3/ZrO_2	219, 240, 251(sh)	5.0	0.1	monotungstate	monotungstate (monoxo WO_5)	distorted WO_4[30,76,77]
4.5 W/nm^2 WO_3/ZrO_2	218, 246, 268 (sh)	4.2	1.9	combination of mono- and polytungstates	polytungstate (monoxo WO_5/WO_6)	distorted WO_5/WO_6[30,76,77]
∼0.1 W/nm^2 WO_3/SiO_2	228, 261	4.2	2.0	monotungstate or combination of mono- and polytungstate	monotungstate (dioxo WO_4)	N/A
∼0.5 W/nm^2 WO_3/SiO_2	235, 270	4.0	2.4	monotungstate or combination of mono- and polytungstate	monotungstate (dioxo WO_4) and polytungstate (monoxo WO_5/WO_6)	N/A

characteristic of monoxo-containing surface WO_5 monotungstates and surface WO_5/WO_6 polytungstates, respectively.[89]

The corresponding UV−vis DRS E_g values under ambient and dehydrated conditions for the 0.5WAl sample are ∼5.3 and ∼5.1 eV, respectively, which are similar in value for reference compounds containing isolated WO_4 units (i.e., Na_2WO_4, Table 3).[46] The presence of only a single LMCT band maximum at 227−228 nm confirms the isolated nature of the supported WO_4 units. The UV−vis DRS E_g values under ambient and dehydrated conditions for the 4.5WAl samples are ∼4.1 and ∼4.0, respectively, and similar to the values found for tungstate reference compounds consisting of either polytungstate WO_x chains (i.e., $Na_2W_2O_7$, alternating WO_4 and WO_6 units, Table 3),[46] highly distorted isolated WO_4 species (i.e., $Al_2(WO_4)_3$ and $Zr(WO_4)_2$), or a mixture of monotungstates and polytungstates. Multiple LMCT transitions are observed for the 4.5WAl sample at ∼228−234 and ∼254 nm under hydrated and dehydrated conditions. The low value of the LMCT transitions at ∼228−234 nm reflects the presence of a slightly distorted isolated surface WO_4 species, and the additional band at ∼254 nm is representative of either a highly distorted monotungstate WO_4 species or a polytungstate species, with the latter more likely.

The combined Raman and UV−vis spectroscopic information suggests the following supported tungstate structures on Al_2O_3 under ambient and dehydrated conditions. The surface WO_x species on Al_2O_3 at low coverage is a slightly distorted monotungstate species under both hydrated ($[WO_4]^{2-}$) and dehydrated ($O_4W{=}O$) conditions. Note that the UV−vis spectral features for such a reference structure are not contained in Table 3 because such a reference compound was not obtained. The hydrated surface WO_x species on AlO_3 at monolayer coverage are present as monotungstate $[WO_4]^{2-}$ and polytungstate $[W_{12}O_{39}]^{6-}$ clusters. The dehydrated surface WO_x species on Al_2O_3 at monolayer coverage are present as both monotungstate and polytungstate WO_5/WO_6 species possessing the monoxo W═O functionality.

Supported WO_3/ZrO_2 Catalysts. The Raman spectra of the supported WO_3/ZrO_2 catalysts under ambient and dehydrated conditions are shown in Figure 5. The ZrO_2 (monoclinic) support possesses strong Raman bands at ∼640, ∼615, ∼558, ∼535, ∼475, ∼380, ∼330, ∼267, and ∼215 cm^{-1} that interfere with the detection of the Raman bands for tungstate vibrations that occur below ∼700 cm^{-1}. Fortunately, no ZrO_2 Raman bands are present in the critical 700−1100 cm^{-1} region where the W═O vibrations for the supported tungsten oxide species occur. A small Raman band from trace amounts of crystalline WO_3 NPS at 816 cm^{-1} is only present in the spectra for the dehydrated 4.5WZr catalyst sample, which reflects the good dispersion of the tungsten oxide phase on the ZrO_2 support. Under ambient conditions where the surface is hydrated, the Raman spectra of the supported 0.5 and 4.5 WZr catalysts exhibit bands at ∼945 and ∼955 cm^{-1} due to the symmetric stretching mode of the hydrated surface WO_x species.[27,40] The hydrated Raman band at ∼945 cm^{-1} at low surface coverage is characteristic of aqueous distorted $[WO_4]^{2-}$, and the band at ∼955 cm^{-1} is most probably a combination of distorted aqueous $[WO_4]^{2-}$ and aqueous $[HW_6O_{21}]^{5-}$ paratungstate.[31] Upon dehydration the major Raman bands associated with the surface tungsten oxide species become sharp and shift from ∼1000 to ∼1010 cm^{-1} with surface WO_x coverage. The appearance of the short W═O bonds at ∼1000 and 1010 cm^{-1} are characteristic of dehydrated surface WO_5 monotungstate and surface WO_5/WO_6 polytungstate species, respectively.[40,88,89] An additional Raman band is present at ∼915 cm^{-1} for the dehydrated monolayer 4.5 WZr catalyst samples from the bridging W−O−Zr bond.[89]

The corresponding UV−vis DRS E_g values under ambient and dehydrated conditions for the 0.5WZr catalyst sample are

~4.6 and ~5.0 eV, respectively, which are similar in value for reference compounds that possess both distorted isolated WO_6 and isolated WO_4 structures (i.e., $NiWO_4$ and Na_2WO_4, respectively, see Table 3).[46] The dehydrated 0.5WZr catalyst sample E_g value corresponds to isolated WO_4 species (see Table 3) or possibly isolated WO_5 species. The corresponding UV−vis DRS E_g values under ambient and dehydrated conditions for the 4.5WZr sample are ~4.3 and ~4.2 eV, respectively, which is similar to the value found for reference compounds consisting of polymeric WO_x chains (i.e., $Na_2W_2O_7$ with alternating WO_4 and WO_6 units in Table 3),[46] dimeric W_2O_7 (i.e., MgW_2O_7 in Table 3), highly distorted isolated species (i.e., $Zr(WO_4)_2$ in Table 3), or even a mixture of slightly distorted WO_4 and polytungstate. The appearance of multiple LMCT transitions at ~221−226 and 249 nm under ambient conditions and LMCT transitions at ~219, 240−246, and 251−264(sh) suggests that both monotungstate and polytungstate species are present for 4.5WZr under all conditions.

The combined Raman and UV−vis spectroscopic information suggests the following supported tungstate structures on ZrO_2 under ambient and dehydrated conditions. Under ambient conditions, only hydrated isolated $[WO_4]^{2-}$ species are present at low coverage and hydrated $[WO_4]^{2-}/[HW_6O_{21}]^{5-}$ species are present at monolayer coverage. Under dehydrated conditions, isolated surface $O_4W{=}O$ monotungstate is found at low coverage and surface WO_5/WO_6 polytungstate species are present at monolayer coverage.

Supported WO_3/SiO_2 Catalysts. The Raman spectra of the supported WO_3/SiO_2 catalysts under ambient and dehydrated conditions are presented in Figure 6. The SiO_2 support possesses weak Raman bands at ~802, ~605, ~490, and ~400 cm^{-1} originating from vibrations of 2-, 3-, and 4-membered silica rings and a band at ~975 cm^{-1} which is associated with the Si−OH vibration.[68,73] A trace amount of WO_3 NPs is present for the hydrated 0.5WSi catalyst sample as revealed by the weak Raman bands at ~807 and ~713 cm^{-1}, which reflects the high dispersion of the tungsten oxide phase on the SiO_2 support under hydrated and dehydrated conditions. Under ambient conditions, Raman bands appear at ~966 cm^{-1} with accompanying bands at lower wavenumbers for the 0.1 and 0.5 WSi catalysts originating from the hydrated $[W_{12}O_{39}]^{6-}$ clusters that have been previously identified on hydrated SiO_2 supports.[29,74] These bands are probably slightly shifted to higher wavenumber values because of the contribution of the of the Si−OH vibration at ~975 cm^{-1}. Upon dehydration, the surface WO_x species give rise to strong Raman bands at 981−985 and 1015 cm^{-1}, with the latter only present for the supported 0.5WSi catalyst. The Raman bands between 980 and 990 cm^{-1} are consistent with a dehydrated isolated surface WO_4 structure with dioxo $O{=}W{=}O$ coordinated species.[89] The Raman band at 1015 cm^{-1} is characteristic of monoxo $W{=}O$ surface WO_5 coordinated species[89] with the weak band at ~346 cm^{-1} assigned to the bending mode of the dehydrated surface WO_4/WO_5 species.

The corresponding UV−vis DRS E_g values for the ambient 0.1 and 0.5WSi are both 4.2 eV, and upon dehydration the E_g values remains about the same (4.0−4.2 eV). Under hydrated conditions, both samples contain two LMCT transition at ~224 and 260 nm, whereas upon dehydration the LMCT transitions slightly shift to 228−235 and 261−270 nm, respectively. Both the LMCT band maxima and the E_g values suggest that the surface tungstate consists of distorted isolated WO_4 dioxo surface species as well as polytungstate monoxo surface WO_5/WO_6 species.

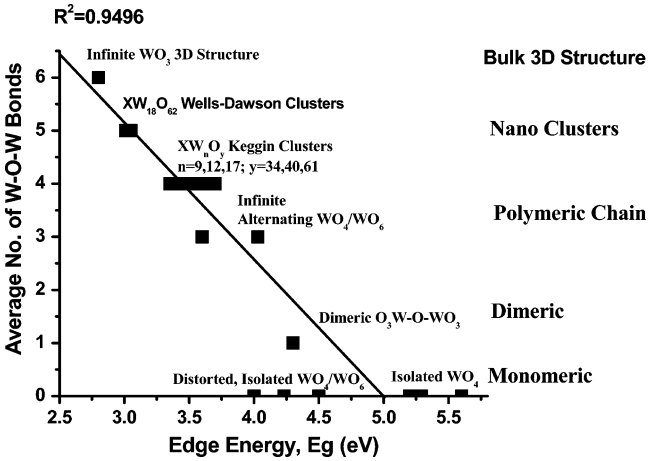

Figure 7. Correlation between the UV−vis DRS edge energy and the average number of bridging W−O−W bonds in bulk tungstates.

The combined Raman and UV−vis spectroscopic information suggests the following supported tungstate structures on SiO_2 under ambient and dehydrated conditions. The ambient WSi catalysts contain both hydrated $[W_{12}O_{39}]^{6-}$ polytungstate and some hydrated $[WO_4]^{2-}$ monotungstate species. Raman is more sensitive to the polytungstate clusters, as well as the WO_3 NPs, and UV−vis detects both surface tungstate species. Under dehydrated conditions, the presence of surface WO_4 dioxo $W(=O)_2$ species is present for at both loadings for the supported WO_3/SiO_2 catalysts, and monoxo polytungstate surface WO_5/WO_6 species are also present for the higher surface coverage 0.5 WSi catalyst sample. The two LMCT bands in the UV−vis spectra indicate that two distinct surface tungstate species are present on the SiO_2 support under all conditions, which reflect the greater sensitivity of UV−vis for isolated surface tungstate species.

4. Discussion

Correlation of the UV−vis DRS E_g with the Local Structures of W(VI) Oxides. The UV−vis DRS edge energies of V(V) and Mo(VI) cations have previously been successfully correlated with the number of M−O−M bonds or the local symmetry of the central cation.[50,52] Qualitatively, the UV−vis DRS edge energies of the W(VI) cation have also been found to be sensitive to the local coordination geometry and cations in the second coordination sphere.[9,10,53] Following the previous successful empirical correlations between E_g and the number of nearest cations surrounding the central M cation, a correlation between E_g and the average number of covalent bridging W−O−W bonds (N_{W-O-W}) of the central W(VI) cation is also examined for the W(VI)-containing tungsten oxide reference compounds of this paper. The plot of E_g vs N_{W-O-W} is presented in Figure 7, where the E_g values linearly vary inversely with N_{W-O-W} with the exception of the isolated WO_x structures whose E_g values vary over a wide range (~4.0−5.6 eV), which is similar to the earlier correlation for V(V) compounds.[50] These relationships are quite similar to the number of next nearest metal neighbors (N_M) proposed by Weber[52] for Mo(VI) compounds, which represents the degree of aggregate/polymerization of the absorbing species. The line shown in Figure 7 can be expressed by the equation

$$N_{W-O-W} = 11.89 - 2.37E_g \text{ with } R^2 = 0.9496 \qquad (1)$$

The high R^2 value is attributed to the distribution of E_g values for the isolated WO_4/WO_5 structures over a wide range (~4.0−

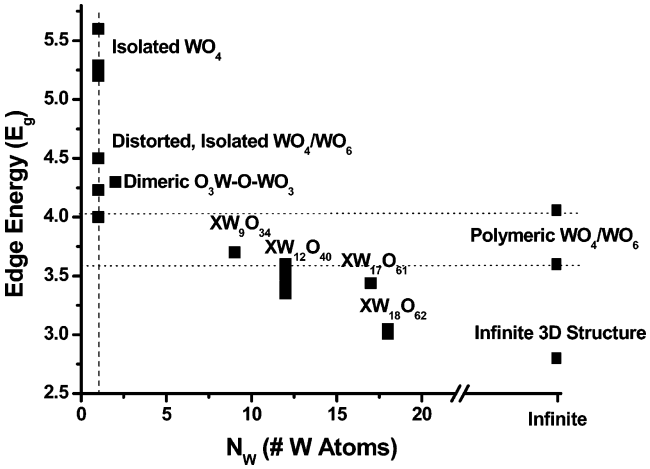

Figure 8. Correlation between the UV−vis DRS edge energy and the number of W atoms (N_W) present in bulk tungstate reference compounds.

5.6 eV) due to the distortion of the isolated WO_x structures. The obtained W(VI) correlation is comparable to that obtained by Weber for Mo(VI) oxide clusters, $N_{Mo} = 16 - 3.8E_g$, and Gao et al. for V(V) oxide clusters, $N_{V-O-V} = 14.03 - 3.95E_g$. The similar correlations obtained for the W(VI), Mo(VI), and V(V) cations suggest that the edge energies of metal oxide clusters are associated with the extent of spatial delocalization of the molecular orbitals involved with electronic transitions, as initially proposed by Weber.[52] It follows from the correlation in Figure 7 that E_g is primarily determined by the number of covalent bridging W−O−W bonds or the degree of polymerization of the central W(VI) cation. The wide range of E_g values obtained for the isolated WO_4/WO_6 structures appears to reflect the sensitivity of the UV−vis DRS measurement to the extent of distortion of W(VI) cation and needs to be considered when determining local structures.

An inverse relationship between E_g and domain size or number of WO_x units in a tungsten oxide cluster has also recently been invoked in the literature[10,40,46,76] but never been rigorously examined. The plot of E_g versus N_W, where N_W represents the number of W atoms present in a finite cluster, is presented in Figure 8. The E_g vs N_W plot does not support a direct relationship between E_g and N_W or domain size for finite WO_x clusters as shown by the plot in Figure 8. First, the E_g values for isolated WO_4/WO_6 structures vary over a very wide range due to the sensitivity to extent of distortion of the W(VI) cation. Second, comparable E_g values are obtained for finite W_9-W_{18} clusters and infinite linear chains. Third, both crystalline WO_3 NPs and polymeric W_2O_7 linear chain structures are infinite but exhibit widely varying E_g values. The inverse relationship between E_g and N_{W-O-W} better captures the variation of the UV−vis DRS E_g values with the local structure of the W(VI) cation.

Surface Structures of Supported Tungsten Oxide Catalysts. The E_g vs N_{W-O-W} correlation implies that the edge energies of the supported tungsten oxide species can also be used to estimate the local WO_x surface structures. The average N_{W-O-W} for the supported tungsten oxide catalysts can be calculated based on the empirical equation obtained above, $N_{W-O-W} = 11.89 - 2.37E_g$, and the results are listed in Tables 4 and 5 with the UV−vis DRS possible structural assignments. However, since the E_g values tend to be rather complex when multiple structures are present, it is necessary to also include the LMCT transitional bands when making structural assignments as well as employ complementary structural characterization results obtained via Raman, IR, and X-ray absorption near-edge spectroscopy (XANES).

Supported WO_3/Al_2O_3 Catalysts. For the hydrated supported 0.5WAl catalyst, <15% monolayer coverage, the current UV−vis and Raman are in agreement with each other and XANES structural studies conducted by Horsley et al.,[30] Eibl et al.,[42] and Hilberg et al.[77] concluding hydrated WO_4 coordinated monotungstate units are present (see Table 4). For the hydrated supported 4.5 WAl monolayer catalyst, the current UV−vis and Raman and previous XANES studies are also in agreement that distorted square pyramidal (WO_5) or pseudo-octahedral (WO_6) structures are the predominant species (see Table 4), with Raman indicating the presence of hydrated $[W_{12}O_{39}]^{6-}$ polytungstate species. UV−vis analysis also suggests the presence of some monotungstate species.

Under dehydrated conditions, all spectroscopic characterization studies are in agreement that isolated surface tungstate species are present for dehydrated 0.5WAl (see Table 5). Raman analysis suggests that the surface monotungstate species possess monoxo W═O functionality (O_4W═O). The presence of dehydrated surface WO_5/WO_6 polytungstate species are concluded for the 4.5WAl catalyst sample from all spectroscopic methods (see Table 5) with the additional observation of isolated monotungstate species from UV−vis DRS.

Supported WO_3/ZrO_2 Catalysts. The assigned tungstate structures on the ZrO_2 support are also in agreement with Raman, UV−vis, and earlier XANES[42] spectroscopic measurements and almost the same as those found above for the supported WO_3/Al_2O_3 catalysts (see Tables 4 and 5). The hydrated polytungstate $[HW_6O_{21}]^{5-}$, however, is found at monolayer coverage on ZrO_2, while the hydrated $[W_{12}O_{39}]^{6-}$ is found for the comparable Al_2O_3 catalyst because of the different pH at point of zero charge (PZC) values of the hydrated supports.

Supported WO_3/SiO_2 Catalysts. Unlike WO_3 supported on ZrO_2 and Al_2O_3 where the catalyst edge energy and average N_{W-O-W} values are a strong function of the tungsten oxide loading, this does not hold true for supported WO_3/SiO_2. The supported 0.1WSi and 0.5WSi catalysts exhibit intermediate edge energies of 4.2 eV under ambient conditions and 4.0−4.2 eV under dehydrated conditions, reflecting N_{W-O-W} values of ~2.0 and ~2.0−2.4, respectively. The UV−vis DRS possess multiple LMCT transitions at ~222 and 260 nm under ambient conditions and ~228−235 and 261−270 nm under dehydrated conditions. Comparison with reference compounds suggests that on the SiO_2 surface highly distorted isolated surface WO_x are the predominate species (i.e., $Al_2(WO_4)_3$ and $NiWO_4$ contain distorted WO_4 and WO_6 units, see Table 3).[46] The correlation results, however, also suggest that the surface WO_x species could lie within the polymeric region. It is for this reason that complementary characterization techniques must be used to verify the molecular species present. In the present study under ambient conditions Raman bands appear at ~966 cm^{-1} with accompanying bands at lower wavenumbers for the 0.1 and 0.5 WSi catalysts originating from hydrated $[W_{12}O_{39}]^{6-}$ clusters that have been previously identified on hydrated SiO_2 supports.[29,31,74] The presence of some hydrated $[WO_4]^{2-}$ is also suggested from UV−vis DRS.

Upon dehydration, the surface WO_x species give rise to strong Raman bands at 981−985 and 1015 cm^{-1}, with the latter only present for the supported 0.5WSi catalyst. The Raman band at 981−985 cm^{-1} is consistent with a dehydrated isolated surface WO_4 structure with dioxo O═W═O coordinated species.[89] The Raman band at 1015 cm^{-1} is consistent with monoxo W═O

surface WO_5/WO_6 coordinated species[89] with the weak band at $\sim$346 cm^{-1} assigned to the bending mode of the dehydrated surface WO_4/WO_5 species.

Recent EXAFS studies of supported WO_3/SiO_2 under ambient conditions proposed that either hydrated polytungstate chains or dodecatungstosilicate Keggin clusters are present.[81] Other researchers also detected small amounts of dodecatungstosilicdic acid in hydrated supported WO_3/SiO_2 catalysts when prepared via wet impregnation.[82−84] Hydrated $H_4SiW_{12}O_{40}$ clusters, however, give rise to a sharp Raman band at $\sim$1001 cm^{-1} (see Figure 2) that is not present for the hydrated supported WO_3/SiO_2 catalysts. Furthermore, hydrated $H_4SiW_{12}O_{40}$ clusters would also give rise to two LMCT bands $\sim$254 and $\sim$323 nm with an E_g value of $\sim$3.4 eV, which are not observed for the present hydrated supported WO_3/SiO_2 catalysts. It is well known for hydrated supported MoO_3/SiO_2 that silicomolybdic acid can form after prolonged exposure to moist environments,[85,86] which suggests that the environmental conditions may not have been the same in all these studies. XANES characterization of coordination for the hydrated or dehydrated surface WO_x species on silica has not appeared in the literature to date.

5. Conclusions

The UV−vis DRS spectroscopic method, with the aid of Raman spectroscopy, was utilized to study the surface structures of molecularly dispersed tungsten(VI) oxide on oxide supports (Al_2O_3, ZrO_2, and SiO_2) under ambient and dehydrated conditions. Under ambient conditions, hydrated surface $[WO_4]^{2-}$, $[HW_6O_{21}]^{5-}$, and $[W_{12}O_{39}]^{6-}$ species were found to be present on the supports, and their relative concentration depends on the surface coverage and pH at PZC of the oxide support. At low surface coverage and dehydrated conditions, isolated surface $OW_4{=}O$ monoxo species are present on Al_2O_3 and ZrO_2, and isolated surface $O_2W(=O)_2$ dioxo species are present on SiO_2. At high surface coverage under dehydrated conditions, monotungstate surface $OW_4{=}O$ and polytungstate WO_5/WO_6 species are present on Al_2O_3 and ZrO_2 and monotungstate surface $O_2W(=O)_2$ and monoxo surface WO_5/WO_6 species on SiO_2. The current study demonstrates that the combination of UV−vis DRS and Raman spectroscopy allows discrimination between surface monotungstate and polytungstate structures as well as WO_3 NPs.

On the basis of various tungsten oxide reference compounds, a correlation of $N_{W-O-W} = 11.89-2.37E_g$ was established between the edge energy, E_g, and the average number of covalent W−O−W bonds around the central W(VI) cations. A direct relationship between E_g and N_W, the number of W atoms in a tungstate cluster, however, is not found because of the strong contribution of local structural distortions in the tungstates.

Acknowledgment. This work was supported by the U.S. Department of Energy-Basic Energy Sciences, Grant DEF-G02-93ER14350. The authors thank Dr. Laura E. Briand for the help in synthesizing the various polyoxotungstate structures.

References and Notes

(1) Thomas, C.L. *Catalytic Processes and Proven Catalysts*; Academic Press: New York, 1970.

(2) Satterfield, C. N. *Heterogeneous Catalysis in Practice*; McGraw-Hill: New York, 1980.

(3) Thomas, J. M.; Thomas, W.J. *Principles and Practice of Heterogeneous Catalysis;* VCH Publishers, Inc.: New York, 1997.

(4) Boyse, R. A.; Ko, E. I. *J. Catal.* **1997**, *171*, 191.

(5) Santiesteban, J. G.; Vartuli, J. C.; Han, S.; Bastian, R. D.; Chang, C. D. *J. Catal.* **1997**, *168*, 431.

(6) Scheithauer, M.; Grasselli, R. K.; Knozinger, H. *Langmuir* **1998**, *14*, 3019.

(7) Hino, M.; Arata, K. *J. Chem. Soc., Chem. Commun*. **1988**, *18*, 1259.

(8) Hino, M.; Arata, K. *Chem. Lett.* **1989**, *6*, 971.

(9) Baertsch, C. D.; Komala, K. T.; Chua, Y.-H.; Iglesia, E. *J. Catal*. **2002**, *205*, 44.

(10) Barton, D. G.; Soled, S. L.; Meitzner, G. D.; Fuentes, G. A.; Iglesia, E. *J. Catal*. **1999**, *181*, 57.

(11) Wivel, C.; Clausen, B. S.; Candia, R.; Morup, S.; Topsoe, H. *J. Catal*. **1984**, *87*, 497.

(12) Grenoble, D. C.; Kim, C. J.; Murrell, L. L. U.S. Patent No. 4,-440,872, 1984.

(13) Murrell, L. L.; Grenoble, D. C.; Kim, C. J.; Dispenziere, N. C. *J. Catal*. **1987**, *107*, 463.

(14) Murrell, L. L.; Kim, C. J.; Grenoble, D. C. U.S. Patent No. 4,-233,139, 1980.

(15) Bernholc, J.; Horsley, J. A.; Murrell, L. L.; Sherman, L. G.; Soled, S. *J. Phys. Chem*. **1987**, *91*, 1526.

(16) Ivin, K. J; Mol, J. C. *Olefin Metathesis and Metathesis Polymerization;* Academic Press: London, 1997.

(17) Baileg, G. C. *Catal. Rev.* **1969** 37.

(18) Wang, Y.; Chen, W.; Yang, W.; Xie, Z.; Xu, W.; Huang, D. *Appl. Catal. A: Gen.* **2003**, *250*, 25.

(19) Verpoort, F.; Bossuyt, A. R.; Verdonck, L. *J. Mol. Catal. A: Chem.* **1995**, *95*, 75.

(20) Chen, J. P.; Yang, R. T. *Appl. Catal. A: Gen.* **1992**, *80*, 135.

(21) Djerad, D.; Tifouti, L.; Crocoll, M.; Weisweiler, W. *J. Mol. Catal. A: Chem.* **2004**, *208*, 257.

(22) Baltin, G.; Koser, H.; Wedlandt, K. P. *Catal. Today* **2002**, *75*, 339.

(23) Ai, M. *J. Catal*. **1977**, *49*, 305.

(24) Wachs, I. E. *Catal. Today* **1996**, *27*, 437.

(25) Thomas, R.; Kerkhof, F. P. J. M.; Moulijn, J. A.; Medema, J.; J. de Beer, V. H. *J. Catal.* **1980**, *61*, 559.

(26) Tiltarelli, P.; Iannibello, A.; Villa, P. *J. Solid State Chem.* **1981**, *37*, 95.

(27) Chen, S. S.; Wachs, I. E.; Murrell, L. L.; Wang, L.; Hall, W. K. *J. Phys. Chem*. **1984**, *88*, 5831.

(28) Biloen, P.; Pott, G. *J. Catal.* **1973**, *30*, 169.

(29) Kim, D. S.; Ostromecki, M.; Wachs, I. E. *J. Mol. Catal. A: Chem.* **1996**, *106*, 93.

(30) Horsley, J. A.; Wachs, I. E.; Brown, J. M.; Via, G. H.; Hardcastle, F. D. *J. Phys. Chem.* **1987**, *91*, 4014.

(31) Ostromecki, M. M.; Burcham, L. J.; Wachs, I. E. *J. Mol. Catal. A* **1998**, *132*, 43. Ostromecki, M. M.; Burcham, L. J.; Wachs, I. E. *J. Mol. Catal. A* **1998**, *132*, 59.

(32) Gielgens, L. H.; Van Kampen, M. G.; Broek, M. M.; van Hardeveld, R.; Ponec, V. *J. Catal.* **1995**, *154*, 201.

(33) Fernandez-Garcia, M.; Martinez-Arias, A.; Fuerte, A.; Conesa, J. C. *J. Phys. Chem. B.* **2005**, *109*, 6075.

(34) Gutierrez-Alejandre, A.; Castillo, P.; Ramirez, J.; Ramis, G.; Busca, G. *Appl. Catal., A: Gen.* **2001**, *216*, 181.

(35) Teoh, L. G.; Shieh, J.; Lai, W. H.; Hung, I. M.; Hon, M. H. *J. Alloys Compd.* **2005**, *396*, 251.

(36) Morandi, S.; Ghiotti, G.; Chiorino, A.; Comini, E. *Thin Solid Films* **2005**, *490*, 74.

(37) Glezos, N.; Douvas, A. M.; Argitis, P.; Saurenbach, F.; Chrost, J.; Livitsanos, C. *Microelectron. Eng.* **2006**, *83*, 1757.

(38) Tarlani, A.; Abedini, M.; Khabaz, M.; Amini, M. M. *J. Colloid Interface Sci.* **2005**, *292*, 486−492.

(39) Youn, M. H.; Kim, H.; Jung, J. C.; Song, I. K.; Barteau, K. P.; Barteau, M. A. *J. Mol. Catal. A: Chem.* **2005**, *241*, 227.

(40) Wachs, I. E.; Kim, T.; Ross, E. I. *Catal. Today* **2006**, *116*, 162.

(41) Kuba, S.; Che, M.; Grasselli, R. K.; Knoezinger, H. *J. Phys. Chem. B* **2003**, *107*, 3459.

(42) Eibl, S.; Gates, B. C.; Knoezinger, H. *Langmuir* **2001**, *17*, 107.

(43) Hernandez, M. L.; Montoya, J. A.; Del Angel, P.; Hernandez, I.; Espinosa, G.; Llanos, M. E. *Catal. Today* **2006**, *116*, 169.

(44) Egues, S.; de Resende, N. S.; Schmal, M. *Stud. Surf. Sci. Catal.* **2002**, *143*, 933.

(45) Gao, B.; Ma, Y.; Cao, Y.; Yang, W.; Yao, J. *J. Phys. Chem. B* **2006**, *110*, 14391.

(46) Barton, D. G.; Shtein, M.; Wilson, R. D.; Soled, S. L.; Iglesia, E. *J. Phys Chem. B* **1999**, *103*, 630.

(47) Gazzoli, D.; Valigi, M.; Dragone, R.; Marucci, A.; Mattei, G. *J. Phys. Chem. B* **1997**, *101*, 11129.

(48) Gutierrez-Alejandre, A.; Ramirez, J.; Busca, G. *Catal. Lett.* **1998**, *56*, 29.

(49) Weckhuysen, B. M.; Schoonheydt, R. A. *Catal. Today* **1999**, *49*, 441.

(50) Gao, X.; Wachs, I., *J. Phys. Chem. B* **2000**, *104*, 1261.

(51) Tian, H.; Ross, E. I.; Wachs, I. E. *J. Phys. Chem. B* **2006**, *110*, 9593.

(52) Weber, R. S. *J. Catal.* **1995**, *151*, 470.

(53) Iglesia, E.; Barton, D. G.; Soled, S. L.; Misea, S.; Baumgartner, J. E.; Gates, W. E.; Fuentes, G. A.; Meitzner, G. D. *Stud. Surf. Sci. Catal.* **1996**, *101*, 533.
(54) Catana, G.; Rao, R. R.; Weckhuysen, B. M.; Van Der Voort, P.; Vansant, E. F.; Schoonheydt, R. A. *J. Phys. Chem. B* **1998**, *102*, 8005.
(55) Okada, K; Morikawa, H.; Marumo, F.; Iwai, S. *Acta. Crystallogr*. **1975**, *B31*, 1200.
(56) Knee, F.; Condrate, R. A. *J. Phys Chem. Solids* **1979**, *40*, 1145.
(57) Finke, R. G.; Rapko, B.; Saxton, R. J.; Domaille, P. J. *J. Am. Chem. Soc.* **1986**, *108*, 2947.
(58) Baronetti, T.; Briand, L. E.; Sedran, U.; Thomas, H. J. *Appl. Catal.* **1998**, *172*, 265.
(59) Gambaro, L. A.; Briand, L. E. *Appl. Catal. A: Gen.* **2004**, *264*, 151.
(60) Briand, L. E.; Thomas, H. J.; Baronetti, G. T. *Appl. Catal. A: Gen.* **2000**, *201*, 191.
(61) Lyon, D.; Miller, W.; Novet, T.; Domaille, P.; Evitt, E.; Johnson, D.; Finke, R. *J. Am. Chem. Soc.* **1991**, *113*, 7209.
(62) Kubelka, P.; Munk, F. *Z. Tech. Phys.* **1931**, *12*, 593.
(63) Delgass, W. N.; Haller, G. L; Kellerman, R.; Lunsford, J. H. *Spectroscopy in Heterogeneous Catalysis*; Academic Press: New York, 1979; p 86.
(64) Hardcastle, F. D.; Wachs, I. E. *J. Raman Spectrosc.* **1995**, *26* (6), 397.
(65) Nakamoto, K. *Infrared and Raman Spectra of Inorganic and Coordination Compounds*; John Wiley & Sons, Inc.: New York, 1986.
(66) Fierro, J. L. G., Ed.; *Metal Oxides: Chemistry and Applications;* CRC Press, Taylor & Francis Group, LLC: Boca Raton, FL, 2006; pp 1−30.
(67) Hardcastle, F. D. Ph.D. Dissertation, Lehigh University, Bethlehem, PA; University Microfilms International, Ann Arbor, MI, 1990.
(68) Hardcastle, F. D.; Wachs, I. E. *J. Mol. Catal.* **1984**, *46*,173.
(69) Chan, S. S.; Wachs, I. E.; Murrell, L. L. *J. Catal.* **1984**, *90*, 150.
(70) Vaidyanathan, N.; Houalla, M.; Hercules, D. M. *Surf. Interface Anal.* **1998**, *26*, 415.
(71) Vaidyanathan, N.; Hercules, D. M.; Houalla, M. *Anal. Bioanal. Chem.* **2002**, *373*, 547.
(72) Vuurman, M. A.; Wachs, I. E. *J. Phys. Chem.* **1992**, *96*, 5008.
(73) Gao, X.; Bare, S. R.; Fierro, J. L.; Banares, M. A.; Wachs, I. E. *J. Phys. Chem. B* **1998**, *102*, 5653.
(74) Kim, D. S.; Ostromecki, M.; Wachs, I. E. *Catal. Lett.* **1995**, *33*, 209.
(75) Weinstock, N.; Schulze, H.; Muller, A. *J. Chem. Phys.* **1973**, *59*, 5063.
(76) Barton, D. G.; Soled, S. L.; Iglesia, E. *Top. Catal.* **1998**, *6*, 87.
(77) Hilbrig, F.; Gobel, H. E.; Knozinger, H.; Schmelz, H.; Lengeler, B. *J. Phys. Chem*. **1991**, *95*, 6973.
(78) a. Chan, S. S.; Wachs, I. E.; Murrell, L. L.; Dispenziere, N. C., Jr. *J. Catal*. **1985**, *92*, 1.
(79) Wells, A. F. *Structural Inorganic Chemistry*; Oxford University: London, 1984.
(80) Nakka, L.; Wachs, I. E. Manuscript in preparation.
(81) Martin, C.; Malet, P.; Solana, G.; Rives, V. *J. Phys. Chem. B* **1998**, *102*, 2759.
(82) Thomas, R.; Moulijn, J. A.; de Beer, V. H. J.; Medema, J. *J. Mol. Catal.* **1980**, *8*, 161.
(83) Van Roosmalen, A. J.; Koster, D.; Mol, J. C. *J. Phys. Chem*. **1980**, *84*, 3075.
(84) Colque, S.; Payen, E.; Grange, P. *J. Mater. Chem.* **1994**, *4*, 1343.
(85) Banares, M. A.; Hu, H.; Wachs, I. E. *J. Catal.* **1995**, *155*, 249.
(86) Kasztelan, S; Payen, E.; Moffat, J. B. *J. Catal*. **1988**, *112*, 320.
(87) Hardcastle, F. D.; Wachs, I. E. *J. Raman Spectrosc.* **1990**, *21*, 683.
(88) Hardcastle, F. D.; Wachs, I. E. *J. Raman Spectrosc.* **1995**, *26* (6), 397.
(89) Kim, T.; Burrows, A.; Kiely, C. J.; Wachs, I. E. *J. Catal*. **2007**, *246* (2), 370.
(90) Lee, E. L.; Wachs, I. E. Manuscript in preparation.
(91) Salvati, L.; Makovsky, L. E.; Stencel, J. M.; Brown, F. R.; Hercules, D. H. *J. Phys. Chem.* **1981**, *85*, 3700.